

# Spin-Orbital States and Strong Antiferromagnetism of Layered $\text{Eu}_2\text{SrFe}_2\text{O}_6$ and $\text{Sr}_3\text{Fe}_2\text{O}_4\text{Cl}_2$

Di Lu,<sup>1,2</sup> Ke Yang,<sup>3,1</sup> Lu Liu,<sup>1,2</sup> Guangyu Wang,<sup>1,2</sup> and Hua Wu<sup>1,2,4,\*</sup>

<sup>1</sup>Laboratory for Computational Physical Sciences (MOE), State Key Laboratory of Surface Physics, and Department of Physics, Fudan University, Shanghai 200433, China

<sup>2</sup>Shanghai Qi Zhi Institute, Shanghai 200232, China

<sup>3</sup>College of Science, University of Shanghai for Science and Technology, Shanghai 200093, China

<sup>4</sup>Collaborative Innovation Center of Advanced Microstructures, Nanjing 210093, China

The insulating iron compounds  $\text{Eu}_2\text{SrFe}_2\text{O}_6$  and  $\text{Sr}_3\text{Fe}_2\text{O}_4\text{Cl}_2$  have high-temperature antiferromagnetic (AF) order despite their different layered structures. Here we carry out density functional calculations and Monte Carlo simulations to study their electronic structures and magnetic properties aided with analyses of the crystal field, magnetic anisotropy, and superexchange. We find that both compounds are Mott insulators and in the high-spin (HS)  $\text{Fe}^{2+}$  state ( $S = 2$ ) accompanied by the weakened crystal field. Although they have different local coordination and crystal fields, the  $\text{Fe}^{2+}$  ions have the same level sequence and ground-state configuration  $(3z^2 - r^2)^2(xz, yz)^2(xy)^1(x^2 - y^2)^1$ . Then, the multiorbital superexchange produces strong AF couplings, and the  $(3z^2 - r^2)/(xz, yz)$  mixing via the spin-orbit coupling (SOC) yields a small in-plane orbital moment and anisotropy. Indeed, by tracing a set of different spin-orbital states, our density functional calculations confirm the strong AF couplings and the easy planar magnetization for both compounds. Moreover, using the derived magnetic parameters, our Monte Carlo simulations give the Néel temperature  $T_N = 420$  K (372 K) for the former (the latter), which well reproduce the experimental results. Therefore, the present study provides a unified picture for  $\text{Eu}_2\text{SrFe}_2\text{O}_6$  and  $\text{Sr}_3\text{Fe}_2\text{O}_4\text{Cl}_2$  concerning their electronic and magnetic properties.

## I. INTRODUCTION

Recently, layered  $\text{AFeO}_2$  ( $\text{A} = \text{Sr}, \text{Ba}, \text{Ca}$ ) oxides with a planar  $\text{FeO}_2$  square lattice were synthesized from  $\text{AFeO}_3$  perovskites via the topochemical reduction [1–4]. They are quite interesting for being an above-room-temperature AF insulator despite their layered structures. Their electronic and magnetic properties are intimately correlated with the spin-orbital states of the constituent Fe ions. In addition, they could be further tuned by doping, pressure, and strain, *etc.* For example,  $\text{SrFeO}_2$  was reported to undergo a pressure-induced spin crossover and an insulator-metal transition, even forming a ferromagnetic (FM) half-metallic state of lasting interest [5].

Low-dimensional magnets have long been of considerable interest. The bilayered  $\text{Sr}_3\text{B}_2\text{O}_4\text{Cl}_2$  ( $\text{B} = \text{Fe}, \text{Co}$ ) [6–8] compounds were also prepared recently. Recently, another bilayered  $\text{Eu}_2\text{SrFe}_2\text{O}_6$  with *ab* planar magnetism was synthesized from the *A*-site-ordered layered perovskite  $\text{Eu}_2\text{SrFe}_2\text{O}_7$  [9]. The temperature dependence of the Mossbauer spectrum and neutron powder diffraction data indicated the onset of G-AF (both intra- and interplane AF couplings) magnetic order at a Néel temperature  $T_N \approx 390\text{--}404$  K for  $\text{Eu}_2\text{SrFe}_2\text{O}_6$  with a HS  $\text{Fe}^{2+}$  configuration. However, with the same HS  $\text{Fe}^{2+}$  configuration and a G-AF magnetic order below  $T_N = 378$  K,  $\text{Sr}_3\text{Fe}_2\text{O}_4\text{Cl}_2$  was reported to have a *c*-axis magnetization [6]. Naturally, several questions arise: why do these

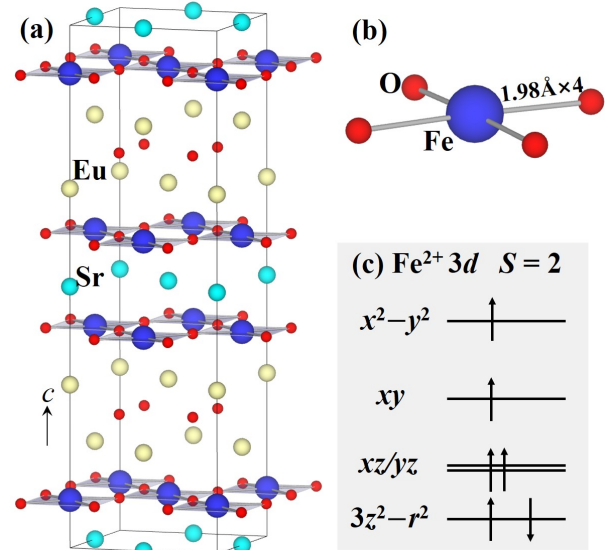


FIG. 1. (a)  $\sqrt{2} \times \sqrt{2} \times 1$  structure of the bilayered  $\text{Eu}_2\text{SrFe}_2\text{O}_6$  with (b) the local 4-fold planar  $\text{FeO}_4$  square. (c) Schematic crystal field level diagrams of the  $\text{Fe}^{2+}$   $S = 2$  state.

two similar bilayered materials with the same HS  $\text{Fe}^{2+}$  charge-spin state have such a contrasting magnetic orientation? Are their orbital states much different to account for this discrepancy? Is there a unified picture to understand their electronic and magnetic properties?

The crystal field diagram is crucial for understanding of the electronic ground state. As seen in Figures 1 and 2, tetragonal  $\text{Eu}_2\text{SrFe}_2\text{O}_6$  and  $\text{Sr}_3\text{Fe}_2\text{O}_4\text{Cl}_2$  both have bilayered structures with  $\text{I4/mmm}$  symmetry. The for-

\* wuh@fudan.edu.cn

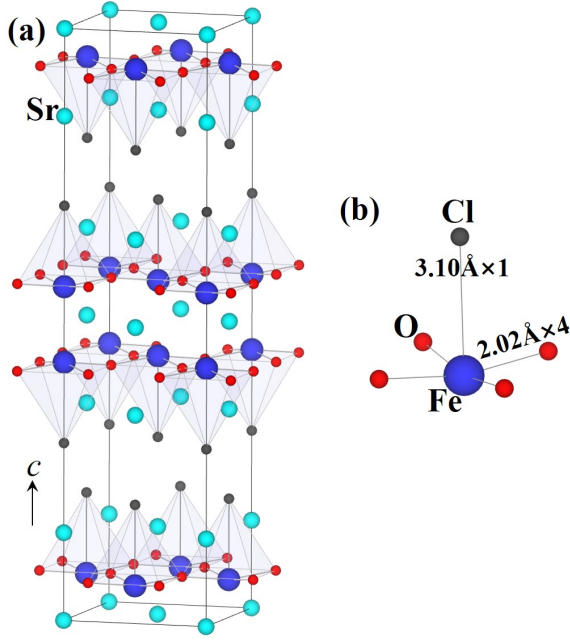


FIG. 2. (a)  $\sqrt{2} \times \sqrt{2} \times 1$  structure of the bilayered  $\text{Sr}_3\text{Fe}_2\text{O}_4\text{Cl}_2$  with (b) the local 5-fold pyramidal  $\text{FeO}_4\text{Cl}$ .

mer has a local 4-fold planar  $\text{FeO}_2$  square lattice, and the  $\text{Fe}^{2+}$  multiple  $d$  states rank in the sequence  $3z^2 - r^2 < xz, yz < xy < x^2 - y^2$ , as shown in Figure 1(c). This level sequence will be confirmed by the following density functional calculations. However, the latter forms a local 5-fold pyramidal  $\text{FeO}_2\text{Cl}$  elongated along the  $z(c)$  axis. Despite the different local structure and crystal field in  $\text{Sr}_3\text{Fe}_2\text{O}_4\text{Cl}_2$ , the elongated Fe-Cl bond along the  $z(c)$  axis provides a similar level sequence as in  $\text{Eu}_2\text{SrFe}_2\text{O}_6$ .

In this work, we study the magnetic and electronic properties of  $\text{Eu}_2\text{SrFe}_2\text{O}_6$  and  $\text{Sr}_3\text{Fe}_2\text{O}_4\text{Cl}_2$  using density functional calculations and Monte Carlo simulations. We find that both materials are Mott insulators, and they have a unified HS  $S = 2$   $\text{Fe}^{2+}$  state with a  $(3z^2 - r^2)^2(xz, yz)^2(xy)^1(x^2 - y^2)^1$  configuration. The orbital mixing between  $(3z^2 - r^2)$  and  $(xz, yz)$  via SOC yields a small in-plane orbital moment and anisotropy. Moreover, the multiorbital superexchanges produce the strong AF couplings. And our Monte Carlo simulations give the  $T_N = 420$  K (372 K) for  $\text{Eu}_2\text{SrFe}_2\text{O}_6$  ( $\text{Sr}_3\text{Fe}_2\text{O}_4\text{Cl}_2$ ), which well reproduce the experimental results. Therefore, our work provides a unified picture to illustrate the electronic and magnetic properties of  $\text{Eu}_2\text{SrFe}_2\text{O}_6$  and  $\text{Sr}_3\text{Fe}_2\text{O}_4\text{Cl}_2$ .

## II. COMPUTATIONAL DETAILS

Density functional theory (DFT) calculations were performed by the full-potential augmented plane waves plus local orbital code (Wien2k)[10]. The optimized lattice

parameters of  $\text{Eu}_2\text{SrFe}_2\text{O}_6$  ( $\text{Sr}_3\text{Fe}_2\text{O}_4\text{Cl}_2$ ) are  $a = b = 3.89$  Å and  $c = 18.80$  Å ( $a = b = 3.96$  Å and  $c = 22.48$  Å), which are close to the experimental values of  $a = b = 3.96$  Å and  $c = 19.01$  Å ( $a = b = 4.01$  Å and  $c = 22.65$  Å) [6, 9]. A  $\sqrt{2}a \times \sqrt{2}b \times c$  supercell is used to treat the intralayer AF configuration. The muffin-tin sphere radii are chosen to be 2.5, 2.0, 1.8, 1.5 Bohr for Eu/Sr, Fe, Cl, and O atoms, respectively. The cutoff energy of 12 Ry is used for plane-wave expansion of the interstitial wave function, and 200  $k$  points are sampled for integration over the first Brillouin zone. The generalized gradient approximation (GGA) [11] by Perdew, Burk, and Ernzerhof (PBE) is employed for the exchange-correlation potential. The SOC is included for the Eu 4*f* and Fe 3*d* orbitals by the second-variational method with scalar relativistic wave functions. Considering the correlation effect of Eu 4*f* and Fe 3*d* electrons, the GGA+SOC+ $U$  [12, 13] method is employed with a common value of  $U = 10$  eV (Hund exchange  $J_H = 0.9$  eV) for the Eu 4*f* electrons [14] and  $U = 5$  eV ( $J_H = 0.9$  eV) for the Fe 3*d* electrons [15]. We examine the charge-spin state and orbital states by crystal field analyses and spin-polarized GGA calculations and then determine the electronic ground state and magnetic anisotropy by GGA+SOC+ $U$ , as detailed below. Moreover, we perform Monte Carlo simulations on  $6 \times 6 \times 1$  and  $20 \times 20 \times 1$  spin matrix by the Metropolis method [16] to estimate the  $T_N$  of  $\text{Eu}_2\text{SrFe}_2\text{O}_6$  and  $\text{Sr}_3\text{Fe}_2\text{O}_4\text{Cl}_2$  using the obtained exchange parameter and magnetic anisotropy from the GGA+SOC+ $U$  calculations.

## III. RESULTS AND DISCUSSION

### A. $\text{Eu}_2\text{SrFe}_2\text{O}_6$

We first examine the electronic properties of  $\text{Eu}_2\text{SrFe}_2\text{O}_6$  by crystal field analyses. As seen in Figure. 1, four  $\text{O}^{2-}$  ions surround the  $\text{Fe}^{2+}$  ion to form the local 4-fold  $\text{FeO}_4$  coordination, and the corner-sharing  $\text{FeO}_4$  comprise a planar square lattice. On the basis of the experimental G-AF state which is also verified by our calculations, the spin-polarized GGA calculations show that Fe 3*d* crystal field level sequence accords with the sketched level diagram, see Figures 1(c) and 3. The  $x^2 - y^2$  orbital has the highest energy and the  $xy$  orbital follows. The  $3z^2 - r^2$  is the lowest due to the planar square  $\text{FeO}_4$  structure (no apical atom). The up-spin 3*d* orbitals are fully occupied, and the down-spin  $3z^2 - r^2$  is also occupied, suggesting the HS  $\text{Fe}^{2+} 3d^6$  state. The O 2*p* states lie mainly at 2-5 eV below the Fermi energy, and they have some hybridization with Fe 3*d* states. The Eu 4*f* states, upon inclusion of the SOC, split into the lower  $J_{\text{eff}} = 5/2$  6-fold states and higher  $J_{\text{eff}} = 7/2$  8-fold states. The fully occupied  $J_{\text{eff}} = 5/2$  states indicate the nonmagnetic  $\text{Eu}^{3+} 4f^6$  state. Owing to the Fe 3*d* exchange splitting and the Eu 4*f* SOC splitting, a small energy gap is already present in the GGA framework.

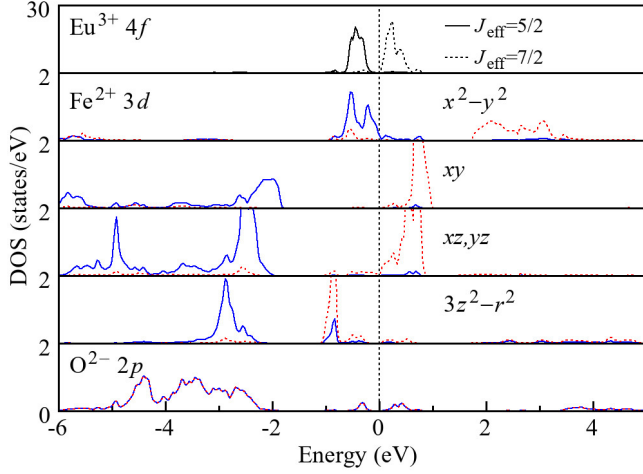


FIG. 3.  $\text{Eu}^{3+} 4f$ ,  $\text{Fe}^{2+} 3d$ , and  $\text{O}^{2-} 2p$  DOS results of  $\text{Eu}_2\text{SrFe}_2\text{O}_6$  in the G-AF ground state by spin-polarized GGA (with inclusion of SOC only for Eu  $4f$ ). Blue (red) curves stand for the up (down) spin channel. Fermi energy is set at zero energy.

Note that  $\text{Eu}_2\text{SrFe}_2\text{O}_6$  is a narrow band system, and its bandwidth around the Fermi level is less than 1 eV. Naturally, its insulating gap would readily be increased when the electronic correlation effect is included as shown below.

We carry out GGA+SOC+ $U$  calculations to address the electronic correlation and SOC effect. To make a direct comparison among the different Fe  $3d$  orbital multiplets, we initialize the corresponding density matrix (and the orbitally dependent potential) and then do a full electronic relaxation in the self-consistent way. On the basis of the G-AF state, the total-energy results of different orbital states with different spin orientations are summarized in Table I. The  $\text{Fe}^{2+} d^{5\uparrow}(3z^2 - r^2)^\downarrow$  state turns out to be the ground state, fully in line with the HS  $S$

TABLE I. Relative Total Energies  $\Delta E$  (meV/Fe), Local Spin, and Orbital Moments ( $\mu_B$ ) of the G-AF, C-AF and A-AF States for  $\text{Eu}_2\text{SrFe}_2\text{O}_6$  by GGA+SOC+ $U$ .<sup>a</sup>

		$\Delta E$	$\text{Fe}^{2+}_{\text{spin}}$	$\text{Fe}^{2+}_{\text{orb}}$
G-AF	$d^{5\uparrow}(3z^2 - r^2)^\downarrow, \parallel$	0	$\pm 3.46$	$\pm 0.07$
	$d^{5\uparrow}(3z^2 - r^2)^\downarrow, \perp$	2.8	$\pm 3.46$	$\pm 0.01$
	$d^{5\uparrow}L_{z+}^\downarrow, \parallel$	879.0	$\pm 3.36$	$\pm 0.03$
	$d^{5\uparrow}L_{z+}^\downarrow, \perp$	852.7	$\pm 3.35$	$\pm 0.80$
C-AF	$d^{5\uparrow}(3z^2 - r^2)^\downarrow, \parallel$	19.3	$\pm 3.43$	$\pm 0.08$
A-AF	$d^{5\uparrow}(3z^2 - r^2)^\downarrow, \parallel$	159.9	$\pm 3.54$	$\pm 0.09$
$J_{ab}=9.99$ $J_c=4.82$ $D=-0.70$				

<sup>a</sup> $\parallel$  ( $\perp$ ) represents the in-plane (out-of-plane) magnetization. The derived exchange and anisotropy parameters (meV) are given.

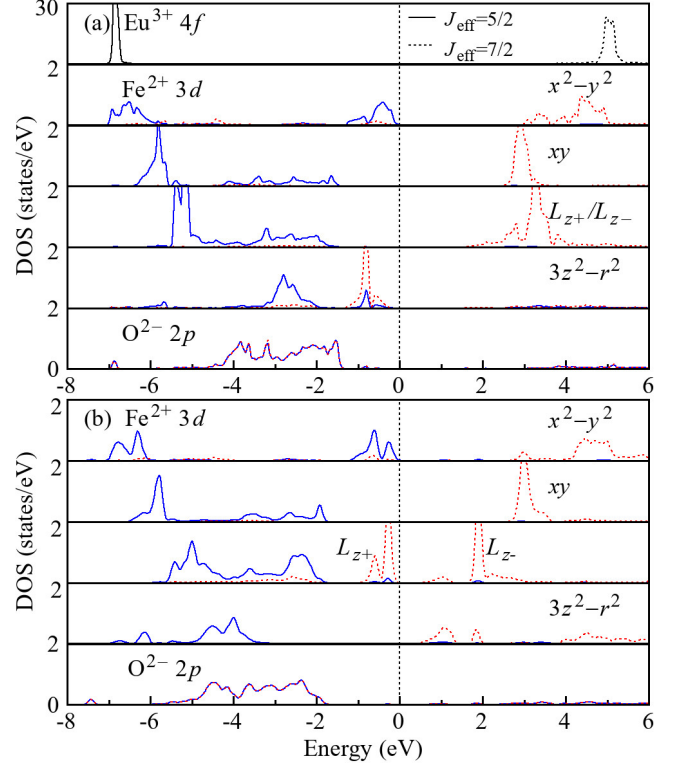


FIG. 4. (a)  $\text{Eu}^{3+} 4f$ ,  $\text{Fe}^{2+} 3d$ , and  $\text{O}^{2-} 2p$  DOS of the  $d^{5\uparrow}(3z^2 - r^2)^\downarrow$  ground state for the G-AF  $\text{Eu}_2\text{SrFe}_2\text{O}_6$  by GGA+SOC+ $U$ ; (b)  $\text{Fe}^{2+} 3d$  and  $\text{O}^{2-} 2p$  DOS of the  $d^{5\uparrow}L_{z+}^\downarrow$  state. Blue (red) curves stand for the up (down) spin channel. Fermi energy is set at zero energy.

= 2 state and the crystal field level sequence with the lowest  $3z^2 - r^2$  orbital. It has the local spin moment of  $3.46 \mu_B$  reduced by the Fe  $3d$ -O  $2p$  hybridization. The DOS results are shown in Figure 4(a): The occupied  $J_{\text{eff}} = 5/2$  states of the  $\text{Eu}^{3+} 4f$  and the unoccupied  $J_{\text{eff}} = 7/2$  states are drastically split due to the very strong electronic correlation of the highly localized  $4f$  orbitals. The  $\text{Fe}^{2+} d^{5\uparrow}(3z^2 - r^2)^\downarrow$  state is also clearly shown, and this Mott insulator has a large band gap of more than 2 eV. As the  $\text{Eu}^{3+}$  ions are nonmagnetic, we need to consider only the  $\text{Fe}^{2+}$  ions for the magnetism of  $\text{Eu}_2\text{SrFe}_2\text{O}_6$ .

When the SOC effect is active, the  $\text{Fe}^{2+} (xz, yz)$  doublet splits into  $L_{z+}$  and  $L_{z-}$  states, with respective orbital moments of  $+1 \mu_B$  and  $-1 \mu_B$  along the  $z$  axis (i.e., the crystallographic  $c$  axis). The SOC mixing between  $(3z^2 - r^2)$  and  $yz$  would produce the  $L_{x+\sqrt{3}}$  and  $L_{x-\sqrt{3}}$  states in the maximum limit with respective orbital moments of  $+\sqrt{3} \mu_B$  and  $-\sqrt{3} \mu_B$  along the  $x$  axis

$$|L_{z\pm}\rangle = \frac{1}{\sqrt{2}}(|xz\rangle \mp i|yz\rangle), \quad (1)$$

$$|L_{x\pm\sqrt{3}}\rangle = \frac{1}{\sqrt{2}}(|3z^2 - r^2\rangle \mp i|yz\rangle).$$

As the crystal field splitting of about 1 eV between the down-spin  $(3z^2 - r^2)$  and  $(xz, yz)$  (see Figure 3)

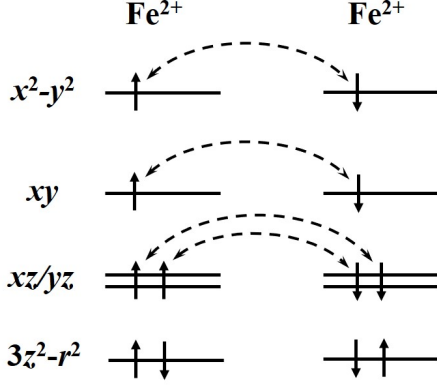


FIG. 5. Schematic crystal field level diagram of  $\text{Fe}^{2+}$   $S = 2$  ions in  $\text{Eu}_2\text{SrFe}_2\text{O}_6$  and  $\text{Sr}_3\text{Fe}_2\text{O}_4\text{Cl}_2$ . Virtual electron hoppings between the neighboring  $\text{Fe}^{2+}$  favor strong AF superexchanges via four channels (the dashed curves).

is much larger than the  $\text{Fe}^{2+}$  SOC strength of about 50 meV, the  $\text{Fe}^{2+}$   $d^{5\uparrow}(3z^2 - r^2)^\downarrow$  ground state carries only a small in-plane orbital moment of  $0.07 \mu_B$  in our GGA+SOC+ $U$  calculation, see Table I. This in-plane orbital moment favors the in-plane magnetization with a magnetic anisotropy energy of 2.8 meV/Fe. This in-plane magnetization is in good agreement with both the experiment results [9] and the prediction by the selection rule based on the SOC-induced HOMO-LUMO interaction. [17] In contrast, we also obtain the  $d^{5\uparrow}L_{z+}$  state as seen in Table I and Figure 4(b). This state has a large orbital moment of  $0.80 \mu_B$  along the  $z$  axis and favors a strong perpendicular magnetic anisotropy of 26.3 meV/Fe (i.e., 879.0-852.7). However, this state lies much higher than the  $d^{5\uparrow}(3z^2 - r^2)^\downarrow$  ground state by 852.7 meV/Fe due to the large crystal field excitation energy from the  $3z^2 - r^2$  orbital to  $(xz, yz)$ .

Now we verify the experimental G-AF ground state of  $\text{Eu}_2\text{SrFe}_2\text{O}_6$ . On the basis of the stable  $d^{5\uparrow}(3z^2 - r^2)^\downarrow$  configuration, we calculate different magnetic configurations (A-AF with intralayer FM and interlayer AF, C-AF with intralayer AF and interlayer FM, G-AF with both intra and interlayer AF) within the GGA+SOC+ $U$ . As seen in Table I, the G-AF ground state is 159.9 (19.3) meV/Fe lower than the A-AF (C-AF) state, implying the strong intralayer (relatively weak interlayer) AF coupling between the neighbouring Fe atoms. Now we explain the G-AF ground state with a high  $T_N$  through the crystal field pictures and intersite orbital interactions. For the magnetic exchange in this Mott insulator, there are four channels for the virtual electron hoppings, see Figure 5 (the doubly occupied  $3z^2 - r^2$  orbital is magnetically inactive). The strongest  $pd\sigma$  hybridization between the Fe  $d_{x^2-y^2}$  and the O  $p_{x,y}$  in the  $ab$  plane produces the strongest intralayer superexchange AF. Another intralayer AF channel is provided by the moderate Fe  $d_{xy} - \text{O } p_{x,y}$   $pd\pi$  hybridization. In addition, the Fe  $d_{xz/yz}$  electrons contribute to the relatively weak intralayer and

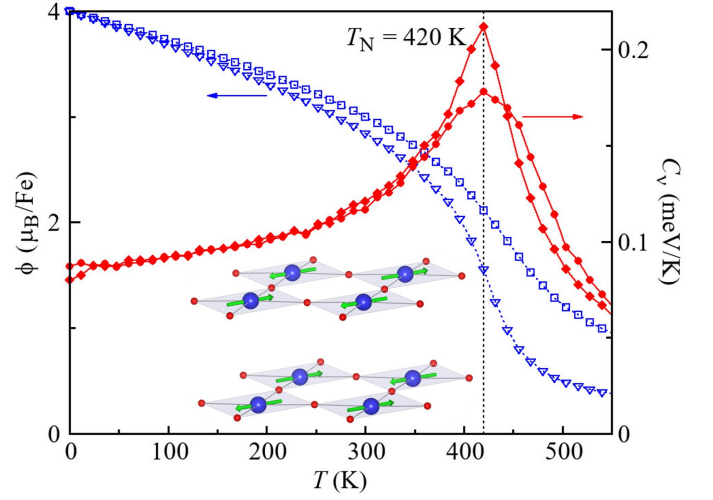


FIG. 6. Monte Carlo simulations of the magnetic specific heat ( $C_v$ ) of  $\text{Eu}_2\text{SrFe}_2\text{O}_6$  and the AF order parameter ( $\phi$ ) using the  $6 \times 6 \times 1$  spin matrix (upper  $\phi$  and lower  $C_v$  curves) and  $20 \times 20 \times 1$  (lower  $\phi$  and upper  $C_v$  curves). (Inset) G-AF ground state in a bilayered unit. Order parameter approaches zero at high temperature with increasing matrix sizes, [18, 19] but estimated  $T_N$  remains unchanged.

interlayer AF couplings. It is this multiorbital AF superexchange which accounts for the experimental high- $T_N$  G-AF state.

By counting the magnetic exchange energy  $-JS^2$  for each AF spin pair with  $S = 2$ , the exchange energies (per Fe) of the three AF states are written as follows

$$\begin{aligned} E_{\text{A-AF}} &= (2J_{ab} - 0.5J_c)S^2, \\ E_{\text{C-AF}} &= (-2J_{ab} + 0.5J_c)S^2, \\ E_{\text{G-AF}} &= (-2J_{ab} - 0.5J_c)S^2. \end{aligned} \quad (2)$$

Using the total energy results in Table I, we obtain the in-plane exchange parameter  $J_{ab} = 9.99$  meV, and the out-of-plane exchange parameter  $J_c = 4.82$  meV. To probe the  $T_N$  of  $\text{Eu}_2\text{SrFe}_2\text{O}_6$ , we carry out Monte Carlo simulations and assume the spin Hamiltonian

$$H = \frac{J}{2} \sum_{\langle ij \rangle} \vec{S}_i \cdot \vec{S}_j - D \sum_i (S_i^z)^2, \quad (3)$$

where the first term denotes the isotropic Heisenberg exchange (AF when  $J > 0$ ) and the second term stands for the single-ion anisotropy [positive (negative)  $D$  for the perpendicular (parallel) magnetic anisotropy]. From the above GGA+SOC+ $U$  result of the easy in-plane magnetization with the anisotropy energy of 2.8 meV/Fe,  $D = -0.70$  meV can be derived. Using the  $J_{ab}$ ,  $J_c$ , and  $D$  parameters, our Monte Carlo simulations of the magnetic specific heat give  $T_N = 420$  K for  $\text{Eu}_2\text{SrFe}_2\text{O}_6$ , see Figure 6, and it is close to the experimental magnetic specific heat of about 400 K [9].

Moreover, to imitate the magnetization (the spontaneous magnetic response in FM materials) for the AF



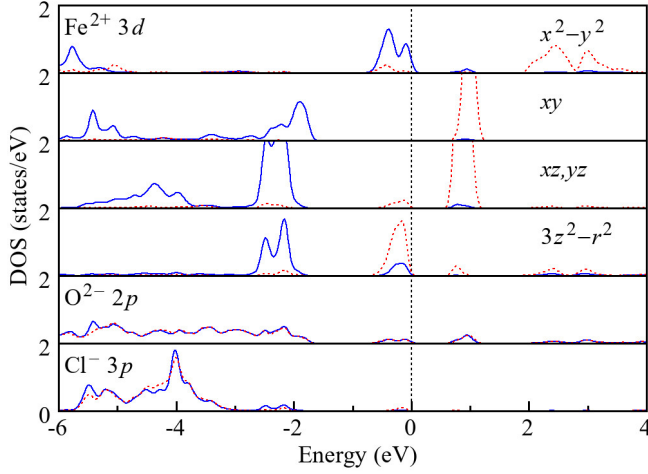


FIG. 7.  $\text{Fe}^{2+}$  3d,  $\text{O}^{2-}$  2p, and  $\text{Cl}^{-}$  3p DOS for the G-AF  $\text{Sr}_3\text{Fe}_2\text{O}_4\text{Cl}_2$  by spin-polarized GGA. Blue (red) curves stand for the up (down) spin channel. Fermi energy is set at zero energy.

$\text{Eu}_2\text{SrFe}_2\text{O}_6$ , we calculate the AF order parameter[18] (the staggered magnetization)

$$\phi = \left| \frac{1}{L^3} \sum_{x=1}^L \sum_{y=1}^L \sum_{z=1}^L (-1)^{x+y+z} \hat{s}(x, y, z) \right|, \quad (4)$$

with  $x$ ,  $y$ , and  $z$  being the integer lattice coordinates of the spins. As shown in Figure 6,  $\phi$  simulates the magnetization of the  $\text{Fe}^{2+}$  ions in G-AF  $\text{Eu}_2\text{SrFe}_2\text{O}_6$  with a saturated magnetic moment of  $4 \mu_B/\text{Fe}$ , and this is in line with the  $\text{Fe}^{2+}$   $S = 2$  state.

TABLE II. Relative Total Energies  $\Delta E$  (meV/Fe), Local Spin, and Orbital Moments ( $\mu_B$ ) of the G-AF, C-AF and A-AF states for  $\text{Sr}_3\text{Fe}_2\text{O}_4\text{Cl}_2$  by GGA+SOC+ $U$ .<sup>a</sup>

		$\Delta E$	$\text{Fe}_{\text{spin}}^{2+}$	$\text{Fe}_{\text{orb}}^{2+}$
G-AF	$d^{5\uparrow}(3z^2 - r^2)^\downarrow, \parallel$	0	$\pm 3.50$	$\pm 0.09$
	$d^{5\uparrow}(3z^2 - r^2)^\downarrow, \perp$	2.6	$\pm 3.50$	$\pm 0.01$
	$d^{5\uparrow}L_{z+}^\downarrow, \parallel$	645.2	$\pm 3.39$	$\pm 0.04$
	$d^{5\uparrow}L_{z+}^\downarrow, \perp$	616.1	$\pm 3.39$	$\pm 0.82$
C-AF	$d^{5\uparrow}(3z^2 - r^2)^\downarrow, \parallel$	27.5	$\pm 3.45$	$\pm 0.10$
A-AF	$d^{5\uparrow}(3z^2 - r^2)^\downarrow, \parallel$	131.7	$\pm 3.56$	$\pm 0.09$
$J_{ab}=8.23$ $J_c=6.88$ $D=-0.65$				

<sup>a</sup>  $\parallel$  ( $\perp$ ) represents the in-plane (out-of-plane) magnetization. The derived exchange and anisotropy parameters (meV) are given.

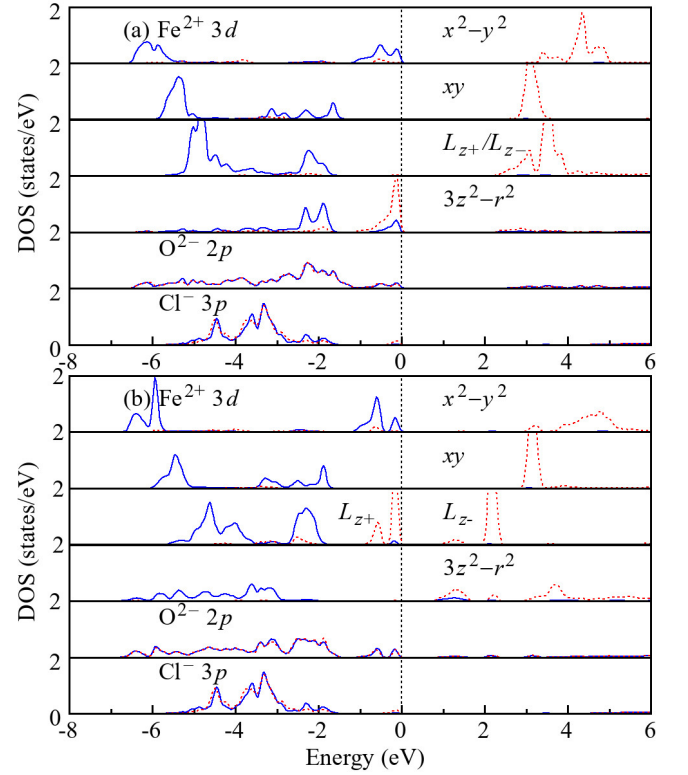


FIG. 8. (a)  $\text{Fe}^{2+}$  3d,  $\text{O}^{2-}$  2p, and  $\text{Cl}^{-}$  3p DOS of  $d^{5\uparrow}(3z^2 - r^2)^\downarrow$  ground state for the G-AF  $\text{Sr}_3\text{Fe}_2\text{O}_4\text{Cl}_2$  by GGA+SOC+ $U$ ; (b)  $\text{Fe}^{2+}$  3d,  $\text{O}^{2-}$  2p, and  $\text{Cl}^{-}$  3p DOS of the  $d^{5\uparrow}L_{z+}^\downarrow$  state. Blue (red) curves stand for the up (down) spin channel. Fermi energy is set at zero energy.

## B. $\text{Sr}_3\text{Fe}_2\text{O}_4\text{Cl}_2$

$\text{Sr}_3\text{Fe}_2\text{O}_4\text{Cl}_2$  has the same tetragonal  $I4/mmm$  symmetry as  $\text{Eu}_2\text{SrFe}_2\text{O}_6$ , but the additional  $z$  axis Cl atom for the  $\text{FeO}_4$  square forms a local 5-fold pyramid. The optimized Fe-O (Cl) bondlengths of 2.02 (3.01) Å are close to the experimental lengths of 2.01 (2.98) Å [6]. The elongated  $\text{FeO}_4\text{Cl}$  pyramid gives a level sequence similar to the case in  $\text{Eu}_2\text{SrFe}_2\text{O}_6$ , see Figures 1 and 2. Indeed, we verify this picture by the spin-polarized GGA calculations, see Figures 3 and 7 for a comparison.

Including the electron correlation and SOC effect, our GGA+SOC+ $U$  calculations find the  $d^{5\uparrow}(3z^2 - r^2)^\downarrow$  G-AF insulating ground state with an easy in-plane magnetization in  $\text{Sr}_3\text{Fe}_2\text{O}_4\text{Cl}_2$ , see Table II and Figure 8(a). It has a local spin moment of  $3.50 \mu_B$  and a small in-plane orbital moment of  $0.09 \mu_B$ , which brings about the magnetic anisotropy of about 2.6 meV/Fe. The  $d^{5\uparrow}L_{z+}^\downarrow$  state [see Figure 8(b)] is now 616.1 meV/Fe higher than the  $d^{5\uparrow}(3z^2 - r^2)^\downarrow$  ground state. This energy difference is smaller than that of 852.7 meV/Fe in  $\text{Eu}_2\text{SrFe}_2\text{O}_6$ , as a consequence of the lifted  $3z^2 - r^2$  level by the additional Fe-Cl bond along the  $z$  axis in the former and of the reduced energy excitation from  $3z^2 - r^2$  to  $(xz, yz)$ . Moreover, by comparing the total energies of the G-AF, C-AF,

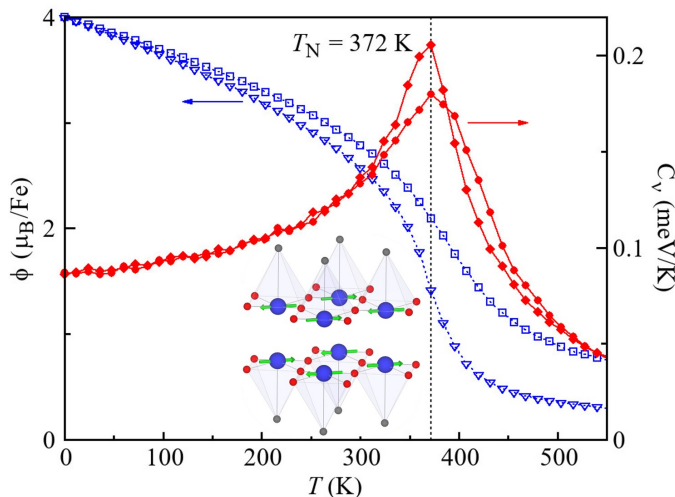


FIG. 9. Monte Carlo simulations of the magnetic specific heat ( $C_v$ ) of  $\text{Sr}_3\text{Fe}_2\text{O}_4\text{Cl}_2$  and the AF order parameter ( $\phi$ ). (Inset) G-AF ground state in a bilayered unit. See more notes in Figure 6.

and A-AF states, we derive the exchange and anisotropy parameters  $J_{ab} = 8.23$  meV,  $J_c = 6.88$  meV, and  $D = -0.65$  meV. Then, our Monte Carlo simulations give  $T_N = 372$  K for  $\text{Sr}_3\text{Fe}_2\text{O}_4\text{Cl}_2$  (see Figure 9), and this is in good agreement with the experimental value of 378 K [6].

Previously, it was found that the bilayered  $\text{Sr}_3\text{Fe}_2\text{O}_4\text{Cl}_2$  has a perpendicular magnetic moment of  $2.82 \mu_B/\text{Fe}$  [6]. We now check this observation carefully. Indeed, we obtain the  $d^{5\uparrow}L_{z+}^\downarrow$  solution with perpendicular magnetization, and it has the spin moment of  $3.39 \mu_B$  per Fe and perpendicular orbital moment of  $0.82 \mu_B$ . The total magnetic moment of  $4.21 \mu_B$  is much larger than the above value of  $2.82 \mu_B$ . However, this solution is significantly higher (by 616.1 meV/Fe) than the  $d^{5\uparrow}(3z^2 - r^2)^\downarrow$  ground state with a small in-plane orbital moment as discussed above. Therefore, the previous observation of the perpendicular magnetic moment of  $2.82 \mu_B/\text{Fe}$  in  $\text{Sr}_3\text{Fe}_2\text{O}_4\text{Cl}_2$  cannot be explained by the present finding. Note that from symmetry analysis, [17] the experimental perpendicular magnetization would most probably arise from the  $\text{Fe}^{2+}$

$d^{5\uparrow}(xz, yz)^\downarrow$  state with the formal  $S_z=2$  and  $L_z=1$ , but the total moment of  $5 \mu_B$  is significantly larger than the experimental value of  $2.82 \mu_B$ . Therefore, the experimental perpendicular magnetic moment [6] of  $2.82 \mu_B$  itself seems to contain inconsistent information, and it was already deemed a contrast to the in-plane magnetization of  $\text{Eu}_2\text{SrFe}_2\text{O}_6$  in another very recent experimental work [9] which leaves this issue open. A similar issue appears recently for several cobaltates containing the HS  $\text{Co}^{2+}$  ions at the axially elongated octahedral sites: [20] a large orbital moment as reported from experiment but a small in-plane orbital moment as predicted by theory. All of these issues may be settled by a further study. It is important to note that our present work provides a unified picture for the electronic and magnetic properties of the bilayered  $\text{Sr}_3\text{Fe}_2\text{O}_4\text{Cl}_2$  and  $\text{Eu}_2\text{SrFe}_2\text{O}_6$  concerning the crystal field level diagram, superexchange AF, easy in-plane magnetization, and high- $T_N$  G-AF order.

#### IV. CONCLUSIONS

In summary, using a set of DFT calculations aided with crystal field and superexchange analyses we find that both  $\text{Eu}_2\text{SrFe}_2\text{O}_6$  and  $\text{Sr}_3\text{Fe}_2\text{O}_4\text{Cl}_2$  are Mott insulators and in the HS  $S = 2$   $\text{Fe}^{2+}$  state. Although they have different local structures and crystal fields, being 4-fold square in the former and 5-fold pyramid in the latter, we find the same level sequence and the  $\text{Fe}^{2+}$   $d^{5\uparrow}(3z^2 - r^2)^\downarrow$  ground state with the easy in-plane magnetization. The multiorbital superexchanges well explain the strong AF couplings in the G-AF ground state. Our Monte Carlo simulations give a high  $T_N = 420$  K (372 K) for  $\text{Eu}_2\text{SrFe}_2\text{O}_6$  ( $\text{Sr}_3\text{Fe}_2\text{O}_4\text{Cl}_2$ ), which well matches the experimental value of  $\sim 400$  K (378 K). Therefore, this work provides a unified picture for the electronic structure and magnetism of  $\text{Eu}_2\text{SrFe}_2\text{O}_6$  and  $\text{Sr}_3\text{Fe}_2\text{O}_4\text{Cl}_2$ .

#### V. ACKNOWLEDGEMENT

This work was supported by National Natural Science Foundation of China (Grants No. 12174062 and No. 12104307).

- 
- [1] Y. Tsujimoto, C. Tassel, N. Hayashi, T. Watanabe, H. Kageyama, K. Yoshimura, M. Takano, M. Ceretti, C. Ritter, and W. Paulus, *Nature* **450**, 1062 (2007).
  - [2] C. Tassel, T. Watanabe, Y. Tsujimoto, N. Hayashi, A. Kitada, Y. Sumida, T. Yamamoto, H. Kageyama, M. Takano, and K. Yoshimura, *J. Am. Chem. Soc.* **130**, 3764 (2008).
  - [3] C. Tassel, J. M. Pruneda, N. Hayashi, T. Watanabe, A. Kitada, Y. Tsujimoto, H. Kageyama, K. Yoshimura, M. Takano, M. Nishi, K. Ohoyama, M. Mizumaki, N. Kawamura, J. Íñiguez, and E. Canadell, *J. Am. Chem. Soc.* **131**, 221 (2009).
  - [4] T. Yamamoto, Z. Li, C. Tassel, N. Hayashi, M. Takano, M. Isobe, Y. Ueda, K. Ohoyama, K. Yoshimura, Y. Kobayashi, and H. Kageyama, *Inorg. Chem.* **49**, 5957 (2010).
  - [5] T. Kawakami, Y. Tsujimoto, H. Kageyama, X.-Q. Chen, C. Fu, C. Tassel, A. Kitada, S. Suto, K. Hirama, Y. Sekiya, *et al.*, *Nat. Chem.* **1**, 371 (2009).

- [6] E. Dixon and M. A. Hayward, *Inorg. Chem.* **49**, 9649 (2010).
- [7] E. Dixon and M. A. Hayward, *Inorg. Chem.* **50**, 7250 (2011).
- [8] F. D. Romero, L. Coyle, and M. A. Hayward, *J. Am. Chem. Soc.* **134**, 15946 (2012).
- [9] S. A. López-Paz, K. Nakano, J. Sanchez-Marcos, C. Tassel, M. Alario-Franco, and H. Kageyama, *Inorg. Chem.* **59**, 12913 (2020).
- [10] P. Blaha, K. Schwarz, G. Madsen, D. Kvasnicka, J. Luitz, R. Laskowski, F. Tran, and L. Marks, “Wien2k software package,” (2001).
- [11] J. P. Perdew, K. Burke, and M. Ernzerhof, *Phys. Rev. Lett.* **77**, 3865 (1996).
- [12] V. I. Anisimov, I. V. Solovyev, M. A. Korotin, M. T. Czyżyk, and G. A. Sawatzky, *Phys. Rev. B* **48**, 16929 (1993).
- [13] V. I. Anisimov, F. Aryasetiawan, and A. Lichtenstein, *J. Phys.: Condens. Matter* **9**, 767 (1997).
- [14] R. Kováčik, S. S. Murthy, C. E. Quiroga, C. Ederer, and C. Franchini, *Phys. Rev. B* **93**, 075139 (2016).
- [15] H. Wang, S. Zhu, X. Ou, and H. Wu, *Phys. Rev. B* **90**, 054406 (2014).
- [16] N. Metropolis and S. Ulam, *J. Am. Stat. Assoc.* **44**, 335 (1949).
- [17] M.-H. Whangbo, E. E. Gordon, H. Xiang, H.-J. Koo, and C. Lee, *Acc. Chem. Res.* **48**, 3080 (2015).
- [18] G. Brown, A. Janotti, M. Eisenbach, and G. Stocks, *Phys. Rev. B* **72**, 140405 (2005).
- [19] N. Crokidakis, D. Soares-Pinto, M. Reis, A. Souza, R. Sarthour, and I. Oliveira, *Phys. Rev. E* **80**, 051101 (2009).
- [20] H.-J. Koo, R. K. Kremer, and M.-H. Whangbo, *Inorg. Chem.* **59**, 18319 (2020).